AIAA JOURNAL
Vol. 54, No. 7, July 2016

Technical Notes

TECHNICAL NOTES are short manuscripts describing new developments or important results of a preliminary nature. These Notes should not exceed 2500 words (where a figure or table counts as 200 words). Following informal review by the Editors, they may be published within a few months of the date of receipt. Style requirements are the same as for regular contributions (see inside back cover).

Test-Model-Induced Interference Effects in Expansion Tube Flows

Yasin M. Abul-Huda* and Mirko Gamba†
The University of Michigan, Ann Arbor, Michigan 48104

DOI: 10.2514/1.J054449

I. Introduction

THE operation of an expansion tube, first introduced by Trimpi [1], relies on a series of unsteady shock and expansion waves to generate a high-enthalpy supersonic flow. This type of flow facility has several advantages over alternative ones in its ability to generate a wide range of high-enthalpy flow conditions. However, the range of accessible flow conditions is ultimately limited by a combination of undesired effects, such as flow disturbances, boundary-layer growth, limited core flow size, and short test times. Previous studies [2–6] have attempted to quantify how some of these effects may alter test conditions and times. Paull and Stalker [3] showed that flow disturbances originating in the driver gas can be transmitted into the test gas, and may undergo a frequency focusing process across the secondary expansion wave [7] to give rise to a significant amplification of pressure fluctuations in the test gas. However, noise transmission to the test gas can be minimized under certain conditions of operation. The presence of the secondary diaphragm has also been found to affect test gas conditions by creating a reflected shock wave that alters the test gas [8,9] and introduces limitations in static pressure measurements [10]. However, the use of thin secondary diaphragms or eliminating them altogether [11] can reduce these undesired effects.

Here we report observations of nonideal operation of expansion tubes that results in undesired properties in the test gas. The interference effects investigated here result from the interaction of the initial unsteady flow with models located in the test section, and induces a significant increase in test gas pressure and temperature at the beginning of the test time. Thus, the experimental flow conditions are altered from what was desired. The test-model-induced interference effect is postulated to be caused by the secondary shock wave diffracting around the test article, generating a series of compression waves that coalesce into an upstream-propagating shock wave, which we refer to as a disturbance wave. In some respect, it is analogous to test model blockage effects in steady flow facilities [12,13]. However, the effects studied here are different from other flow disturbances discussed previously; they also differ from test gas composition contamination in expansion tubes [6] and reflected shock tunnels [14–16].

Under certain operating conditions with test models mounted inside the test section, a strong distortion of the test gas pressure time history measured in the test section (e.g., on models) has been observed, which effectively reduces the test time and alters the aerothermodynamic flow properties from what was desired. Figure 1 shows the static pressure measured in the test section for a typical case where this effect is observed. The static pressure was measured with a flush-mounted PCB piezoelectric transducer inserted in a flat plate with the leading edge protruding 2.1 cm into the expansion section. After the initial phase, where the secondary shock (I) and shocked expansion gas arrive (II), there is a rapid increase in pressure at the end of the expansion gas flow, which results in what we here denote as the secondary overshoot. This is then followed by the test gas with an additional rapid increase in pressure (III) to a peak value approximately two times the design flow pressure, here denoted as the primary overshoot. Subsequently, the pressure decays to the nominal design value (IV) until the arrival of the test time termination wave.

A generalized space–time diagram summarizing the wave processes responsible for altering the test gas properties is shown in Fig. 2. The labeling of the states follows that of Trimpi [1]. After the secondary shock (W_2) arrives in the test section, a disturbance wave (W_U) processes the shocked expansion gas and interacts with the contact surface at a distance $\hat{x}$ from the secondary diaphragm. This results in generating two new waves, a transmitted and a reflected wave. The transmitted wave processes a portion of the test gas and thus alters its aerothermdynamic properties, which causes the primary overshoot in Fig. 1 and is denoted as (5c) in Fig. 2. Furthermore, the interaction reduces the speed of the contact surface, which further limits the useful test time. The reflected wave, which processes the shocked expansion gas, is responsible for the secondary overshoot in Fig. 1 and is denoted as (20b) in Fig. 2.

In this study we investigate the mechanism for the onset of such flow disturbance using a combined experimental, computational, and analytical approach. A series of experiments and computer simulations using ANSYS CFX was carried out to gain insight on the cause of the pressure overshoots and reach the conclusions summarized in Fig. 2. An analytical model describing the observed effects is formulated and is shown to be a useful tool in predicting the extent of test gas interference. Lastly, we provide a brief discussion on what is required to limit the undesired interference effects.

II. Experimental Methodology

A series of experiments was conducted to discern the cause of the pressure overshoot upon arrival of the test gas. Some of the experiments were carried out in the expansion tube facility at Stanford University [17], whereas others in the Michigan Hypersonic Expansion Tube Facility [18,19] (MHExT). The only geometric difference between the two facilities relevant to this study is the inner radius of the tube R, which is 7 and 7.2 cm for the Stanford and Michigan facilities, respectively.

Figure 3 provides a schematic drawing of the assembly that was fixed in the test section to measure the test gas pressure. It is composed of a flat plate with a sharp leading edge instrumented with flush-mounted PCB piezoelectric pressure transducers (Model 113B21).

Received 5 May 2015; revision received 16 November 2015; accepted for publication 31 January 2016; published online 28 April 2016.

*Graduate Research Assistant, Department of Aerospace Engineering; yasinma@umich.edu. Student Member AIAA.

†Assistant Professor, Department of Aerospace Engineering; mirkog@umich.edu. Member AIAA.

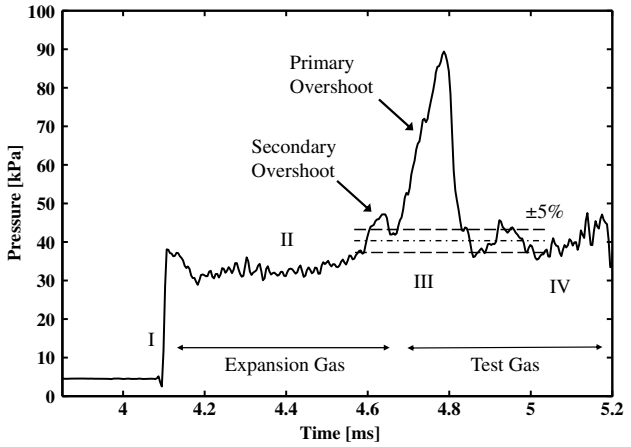

Fig. 1 Static pressure measured on a flat plate mounted inside of the test section under nonideal operation of an expansion tube facility. Condition pertains to Run 2 in Table 1.

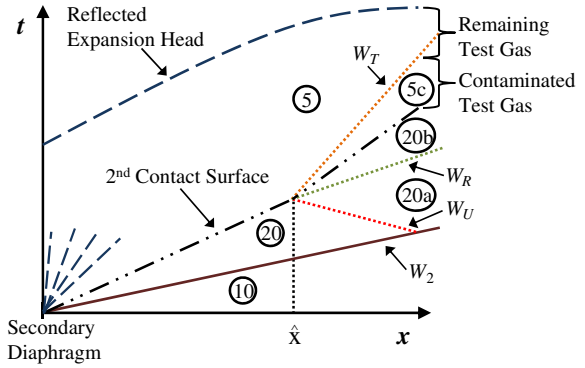

Fig. 2 Generalized space–time diagram of the unsteady wave process responsible for changes in test gas properties. State labels after Trimpi [1].

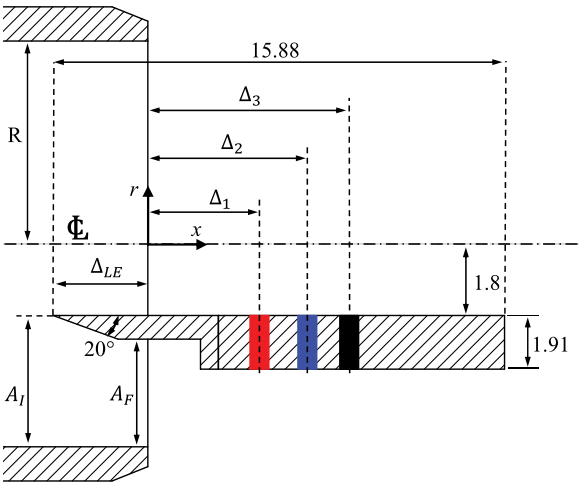

Fig. 3 Schematic of the experimental assembly in the protruding configuration. Dimensions are given in centimeters.

In the Stanford facility, the flat plate was instrumented with three transducers, whereas in the Michigan facility only one transducer was used. The position of the leading edge of the flat plate from the tube exit is given by Δ_{LE}; the resulting distance of each sensor from the tube exit is Δ_i ($i = 1, 2, 3$ for each of the three sensors). The origin is taken to be on the centerline at the exit plane of the tube. Both facilities used a geometrically similar configuration of the flat plate assembly. The span of the plate is 10.2 cm. Two flow conditions, referred to as A and B in Table 1, were considered, and differed in M_{20} (flow Mach number of the shocked expansion gas), which was designed to be greater or less than unity, and M_{W_2}, which is the Mach number of the secondary shock wave. Both conditions used air and helium as the test gas and expansion gas, respectively. They were run with the assembly configured either with the leading edge protruding ($\Delta_{\mathrm{LE}} < 0$) or recessed ($\Delta_{\mathrm{LE}} > 0$) from the expansion tube exit. The different cases are summarized in Table 1. Separate experiments simultaneously measuring pitot and static pressures were carried out to establish the temporal evolution of the flow and determine the arrival of the secondary contact surface marking the start of the test time. For these measurements, a setup similar to that of [10,18,19] was used. More details on the characterization of condition A are reported in [20].

III. Numerical Methodology

The experimental results were modeled with a representative two-dimensional domain using the commercial software ANSYS CFX. Here we consider a two-dimensional representation of the problem to generate a qualitative approximation of the system of waves generated by the presence of a test model, thus providing us with an initial view of the controlling physical processes without any expectation of replicating our experimental observations with much fidelity. The two-dimensional calculations were not intended to fully describe the exact details of the experiments, and certainly do not capture the complexity of the actual (three-dimensional) problem. The flow was modeled as inviscid because the phenomenon of interest was not believed to be governed by viscous effects. In fact, because the magnitude of the observed interference effects on test gas conditions is so large and because wave propagation is considered to be at the root of the observed phenomenon, it was believed that the overall driving mechanism remains inertia-dominated with viscous effects having no effect on the onset of these disturbances but at most affecting their evolution over long times.

The inlet and outlet boundary conditions were supersonic, whereas all walls were imposed with a free slip boundary condition. A second-order backward Euler transient scheme was used and the mesh was composed of cells with dimensions 3 mm × 3 mm. The solution used the NASA polynomials [21] to compute the thermodynamic properties of the gas assuming an equilibrium thermally perfect gas model. Solution convergence was determined by ensuring that 1) the solution was grid independent, and 2) the RMS residual for the mass, momentum, and energy equations decreased by at least 3 orders of magnitude.

Figure 4 shows the domain that was modeled. It includes the test section, flat plate, and a portion of the expansion section. The domain was initialized with axial profiles for velocity, mass fraction, pressure, and temperature and with uniform properties in the cross-sectional direction. For each of the two conditions, the initial values were precomputed from experimentally measured shock speeds and initial fill pressures using an expansion tube solver similar to that of Trimpi [1] and includes equilibrium temperature-dependent properties. The precomputed inlet boundary conditions were kept uniform across the inlet plane. Property changes across the secondary shock wave and contact surface were approximated with error function profiles with an initial thickness of 0.5 and 2 cm, respectively. The

Table 1 Summary of the experimental and numerical test matrix

Run number	Flow condition	M_{W_2}	M_{20}	Δ_{LE}	Δ_i	R, cm
1	*A*	2.6	0.95	0.06	1.01, 1.29, 1.56	7.0
2	*A*	2.6	0.95	−0.49	0.47, 0.74, 1.01	7.0
3	*A*	2.6	0.95	0.11	1.06	7.2
4	*A*	2.6	0.95	−0.46	0.49	7.2
5	*B*	3.5	1.1	0.11	1.06	7.2
6	*B*	3.5	1.1	−0.46	0.49	7.2

The subscript 20 refers to the shocked expansion gas [1]. The distances given by Δ_{LE} and Δ_i are normalized by the inner tube radius R.

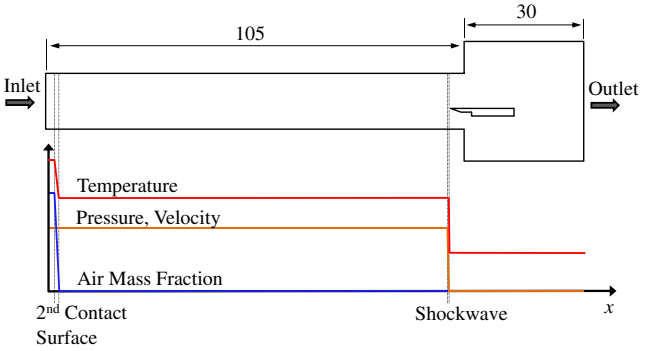

Fig. 4 The two-dimensional CFX domain with a qualitative description of its initialization. All units are in centimeter.

final solution and conclusions of this study were not found to be sensitive to the initial thickness of these features.

IV. Results

The measured surface pressure for Runs 1 and 2 (case A) is provided in Figs. 5a and 5b (solid lines), respectively. These measurements were conducted in the Stanford facility. The corresponding numerical solution is also shown for comparison (symbols). For both cases, the value of M_{20} is slightly less than unity (Table 1). The leading edge is recessed into the test section in Run 1 and protrudes into the expansion tube in Run 2. For each case, all three traces, which are the wall-static pressure measurements at three downstream positions from the leading edge of the flat plate, are observed to share a similar qualitative behavior. The arrival of the secondary shock wave results in the initial step-change in pressure (label I). After the shock wave sweeps past the model, the shocked expansion gas follows (label II), whereas in the expansion section, the flow in state (20) is nearly sonic with $p_{20} > p_{10}$; thus, as the expansion gas further expands into the test section, it behaves as an underexpanded near-sonic jet with a pressure ratio of about 10. The decreasing trend of the measured pressure at different points along the plate (compare curves for different sensor locations in region II) is consistent with the decrease in pressure in the barrel shock of an underexpanded sonic jet [22,23].

The arrival of the secondary contact surface is at the end of region II. At this time, the measured pressure gradually increases, indicating an evolution in the flow. This is caused by the combination of the finite thickness of the contact surface [24,25], the inherent transient evolution associated with the change in flow structure from the barrel shock of the initial underexpanded near-sonic expansion gas to the final underexpanded supersonic test gas flow (IV), and the limited response time of the piezoelectric sensors. However, in the case of Fig. 5b, where the leading edge of the plate protrudes into the expansion tube, there is a region of flow labeled as III, which exhibits a pressure approximately twice that of the designed test gas pressure (i.e., at IV). For this particular case, the contaminated portion of the test gas (referred to as the primary overshoot) extends for approximately 50% of the total test time, rendering the flow condition of limited use. There is also a less pronounced increase in pressure just before the primary overshoot, which is referred to as the secondary overshoot, and takes place within the shocked expansion gas in state (20b). Finally, by comparison of the gas in region II, it is clear that the gas in region II of Fig. 5b is greater than that of Fig. 5a, which is evidence that the expansion gas is further shock-processed in the protruding case.

To ascertain that the observed effects were not facility dependent, flow condition A was replicated in the MHExT facility. These measurements are Runs 3 and 4, and are shown in Fig. 6. We observe the primary and secondary pressure overshoots in the second facility as well. The primary overshoot contaminates approximately 60% of the test gas. The results support our belief that the observed interference effect is independent of the expansion tube facility, but is related to test model interference during the onset of the shocked expansion gas flow. This hypothesis was further investigated through the numerical experiments.

Qualitatively, the numerical solutions (symbols in Figs. 5a and 5b) replicate the same behavior as was observed in the experiments. The quantitative differences between the experimental and numerical solutions presented in Figs. 5a and 5b are attributable to a number of reasons. First, the difference in pressure in region II is believed to be a result of the simulations being two-dimensional, which will form a barrel shock structure that is not equivalent to that of a three-dimensional under-expanded jet of the same jet pressure ratio. This can be seen by comparing the work of [22,23,26], where two- and three-dimensional underexpanded jet structures were experimentally investigated over a wide range of pressure ratios. The two-dimensional jet yields a barrel shock structure with a Mach disk location that is further downstream of the exit plane as compared with a three-dimensional jet, for the same pressure ratio. Therefore, a larger pressure in region II of the CFD simulations as compared with the experiments is to be expected. Second, there is a difference in the peak value of the pressure overshoot in the contaminated test gas. This may be attributed to the simulations being two-dimensional and the actual area blockage by the test article in the test section not being adequately represented in the simulations. For example, in the experiments the flat plate does not span the entire inner diameter of the tube. Moreover, the plate is fixed to the test section floor through a pair of struts, effectively increasing flow blockage. As a result, there are three-dimensional effects present in the experiments that are not accounted for in the simulations. Nevertheless, the simulations capture the same qualitative

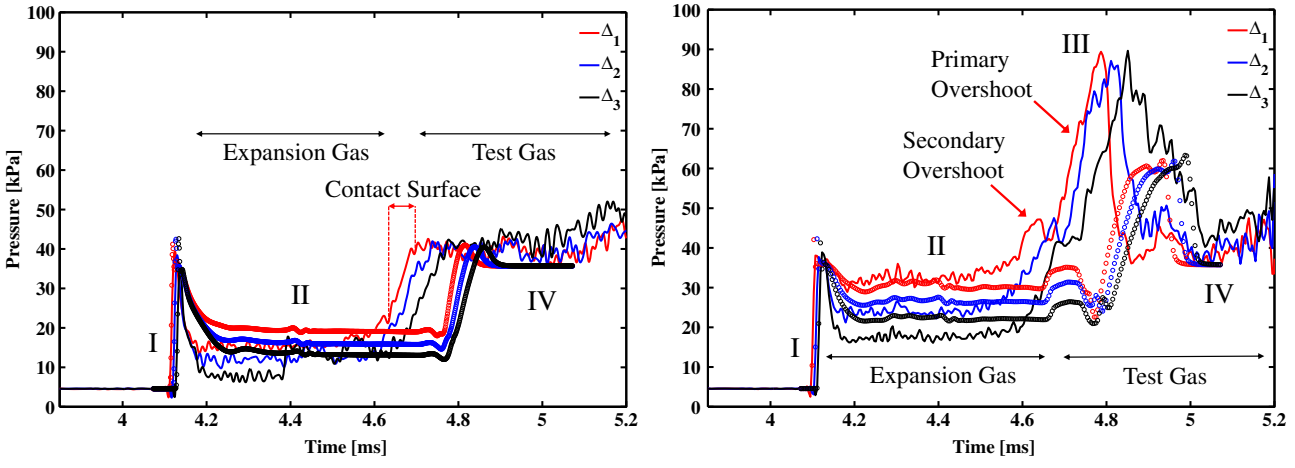

a) b)

Fig. 5 Comparison of experimental (solid) and computational (symbol) pressures for flow condition A. a) Recessed (Run 1) and b) Protruding (Run 2).

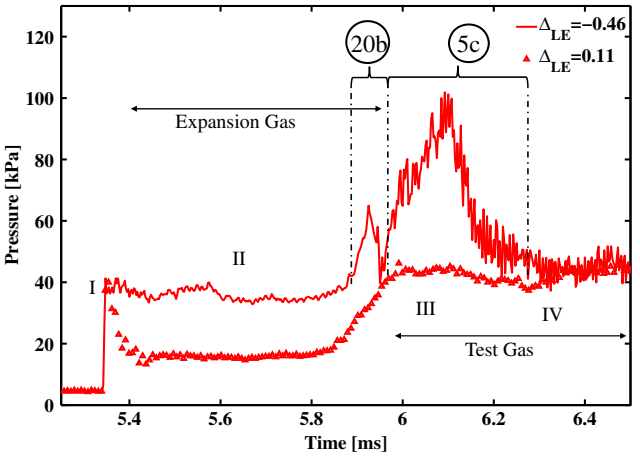

Fig. 6 Experimentally measured pressures for the recessed (Run 3) and protruding (Run 4) configurations for flow condition A.

behavior as was obtained experimentally, providing indication of possible causes of the test gas interference effect.

The numerical and experimental results show that the adverse effects of test gas interference are avoided if the leading edge of the plate does not protrude into the expansion section. To further evaluate the nature of the disturbance, and specifically to ascertain its strength, a second flow condition (B) was designed such that a stronger secondary shock was generated and $M_{20} > 1$. In this case with the flow being supersonic, the upstream propagation of compression waves (relative to the flow) would be altered. The results of the protruding (Run 5) and recessed (Run 6) cases for flow condition B are shown in Fig. 7. The results show that a portion of the test gas is still affected by the interference effect. Therefore, the disturbance wave must be supersonic relative to the flow in state ⑳. Unlike the case with $M_{20} < 1$, the pressure trace in region II for the protruding configuration is not the same as the corresponding one for the recessed configuration. The difference is postulated to be the result of flow compression by a steady detached shock that forms in front of the leading edge of the plate. Finally, based on the results of separate experiments using a pitot-static probe assembly, the measured change in pressure over the test time (IV) for condition B is an undesired characteristic inherent to the flow condition itself and not a result of the interference effect being discussed here.

The numerical solution was used to further explain the link between the observed interference and a possible underlying wave system. A series of pressure contours of the partial domain at relevant time steps for condition A is provided in Fig. 8. The variable t corresponds to the time elapsed from the arrival of the secondary shock wave at the leading edge of the flat plate. The plot beneath each contour represents the air mass ratio along the centerline of the two-dimensional space, indicating the location of the contact surface. The air mass ratio is defined as the relative amount of air at any point in the domain and it is used to differentiate between fluid that originates from state ⑤ from fluid that originates from state ⑳. The series of contours show that the secondary shock separates around the test model. The portion of the shock propagating on top of the flat plate is observed to sweep past the model without generating any upstream propagating disturbances. On the other hand, the portion of the shock propagating beneath the plate diffracts around the leading edge of the test model as it continues through the contracted area [27]. The diffracted portion of the wave coalesces into a finite-strength shock wave at $t = 30$ μs. After an initial formation period ($t = 150$ μs), which originates underneath the test model, the disturbance wave grows to envelop the entire area of the tube and propagates at a speed W_U, in the shock reference frame. As it propagates upstream, it processes the shocked expansion gas from state ⑳ to state ⑳a until it reaches the contact surface at $t = 500$ μs. The wave is then partially reflected and transmitted through the contact surface at $t = 530$ μs. The reflected wave (moving at a speed W_R) is swept downstream, where it further processes the expansion gas from state ⑳a to ⑳b. The portion of the expansion gas in state ⑳b corresponds to the secondary overshoot. At the same time, the transmitted wave (propagating at a speed W_T) propagates through a portion of the test gas, processing it from state ⑤ to ⑤c, as it is swept downstream at $t = 670$ μs. The result is a slug of test gas convected into the test section with a significant portion having different aero-

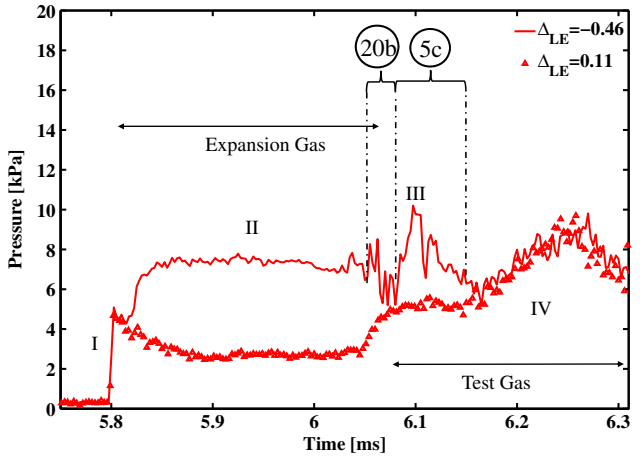

Fig. 7 Experimentally measured pressures for the recessed (Run 5) and protruding (Run 6) configurations for flow condition B.

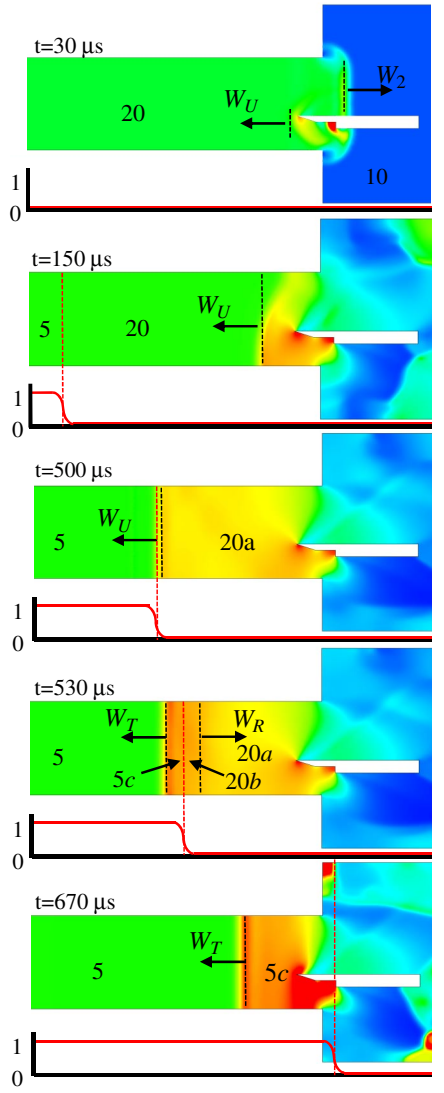

Fig. 8 Pressure contours generated with CFX for Run 2 illustrating the wave processes leading to test gas contamination.

thermodynamic properties than what was originally intended. The primary overshoot is the signature of this portion of the test gas.

V. Modeling

A one-dimensional unsteady wave model of the unsteady process controlling the interaction was constructed to quantitatively predict the impact of the wave system on the final test gas conditions. Modeling of the test gas interference effect was done in two parts. The first portion describes the formation of the disturbance wave as a function of several test parameters, whereas the second portion describes its interaction with the contact surface. The analysis and numerical results of this section are specific to helium as the expansion gas and high temperature air ($\gamma_5 = 1.30$) as the test gas, but they can be readily adapted for any test gas/expansion gas combination.

A. Formation of the Disturbance Wave

Based on the results of the CFX simulations, it was believed that the origin of the disturbance wave was a result of the interaction of the secondary shock wave with the test model. Specifically, it was found that the wave diffracts around the leading edge of the test model as a result of the area contraction it was propagating through [27]. The diffraction process leads to a modified secondary shock wave as well as generates waves that coalesce into an upstream propagating disturbance.

There has been an abundance of work studying the effects of shock-wave propagation through a channel of varying area. The majority of the studies were primarily aimed toward analyzing and optimizing a gradual change in area in order to optimally strengthen the incident shock wave in a shock tube without increasing energy requirements. In particular, the work of Chester [28], Chisnell [29], and Whitham [30] studied the effects of a shock as it propagated through a monotonically varying area change. Using different methods, they individually obtained a similar relation for the strength of a shock wave as a function of the cross-sectional area of the channel it was propagating through. Russel [31] and Bird [32] experimentally investigated the interaction of normal shock waves with symmetrical nozzles of varying geometry. They showed that the gain in shock strength depended on the rate of area change.

In this study, we are interested in capturing the change in shock strength of the secondary shock and the formation of additional (e.g., reflected) waves as it passes through a constriction. Because the area change in which the secondary shock propagates through is not monotonically changing, we adopt the model outlined by Laporte [33]. A schematic of the one-dimensional model is shown in Fig. 9. The secondary shock propagates at a speed W_2 in a channel of initial cross-sectional area A_I through a contracted area of A_F. In our case, the areas correspond to the initial and final cross-sectional areas beneath the leading edge, as indicated in Fig. 3. Upon reaching the constriction, a new set of waves is generated that include a strengthened transmitted wave and a reflected wave propagating at speeds W_3 and W_U, respectively. This interaction forms a region of changing entropy and is shown as the gray region of gas convecting downstream. This region of varying entropy is formed as a result of being shocked by the transmitted wave of incrementally increasing strength as it propagates through the area contraction. As a result, the gas in state (30) and (40) will have the same speed and pressure, but have different entropies, temperatures, and densities. The strengthened wave processes the expansion gas initially in state (10) to state (30), whereas the reflected wave processes the expansion gas from state (20) to (20a). Finally, we approximate the gas as being isentropically compressed from state (20a) to (40). This is valid as long as the angle of the contraction is sufficiently less than 90° and the flow in state (40) remains unchoked. The flow in state (40) chokes as a result of the combination of the secondary shock strength being sufficiently large and the area constriction being sufficiently small. In this case, the Mach number of the flow in state (40) is fixed to unity because an aerodynamic throat would be required to accelerate it to supersonic speeds.

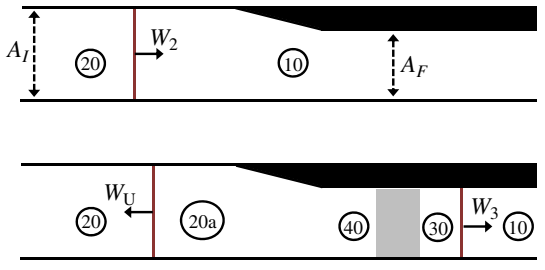

Fig. 9 Schematic drawing of the resulting unsteady wave process generated by the interaction of a shock wave with a sudden contraction.

The upstream propagating disturbance in the present study is the reflected wave in this model. Given the strength of the secondary shock (i.e., W_2), the strength of the upstream propagating disturbance is found using the solution of moving normal shocks and isentropic flow [34] by coupling the solution of the reflected (disturbance) wave with the solution of the strengthened transmitted wave and assuming isentropic compression across the constriction (from (20a) to (40)). This model closely follows the solution of Laporte [33] for a similar configuration. In the case the flow in region 40 reaches the sonic limit (choked), the model remains the same except for the additional condition that the Mach number in state (40) is unity.

This analysis was implemented for helium and is shown in Fig. 10. The strength of the disturbance wave given by P_{20a}/P_{20} is shown as a function of area ratio (A_I/A_F) for multiple secondary shock strengths (p_{20}/p_{10}). The strength of the upstream-propagating wave increases with increasing secondary shock strength and decreasing area-ratios. The Mach number of the wave is in the shock reference frame and is given by

$$M_{W_U} = \frac{U_{20} + W_{U_{\text{lab}}}}{a_{20}} \tag{1}$$

where $W_{U_{\text{lab}}}$ is the wave speed in the lab reference frame. In the limit $A_I/A_F \to 0$, the solution of a shock wave reflected by a wall is found (i.e., the reflected shock tube problem).

Based on this model, we conclude that any combination of secondary shock strength and area contraction will generate a disturbance wave of sufficient strength to propagate upstream. In other words, a condition cannot be designed such that U_{20} is sufficiently large to sweep the disturbance wave downstream. This is in agreement with the experimentally observed results of flow condition 2, where M_{20} was designed to be supersonic, yet the test gas interference effect was still observed.

B. Interaction of Disturbance Wave with the Contact Surface

Upon reaching the contact surface, which is modeled as a zero-thickness material discontinuity, the disturbance wave is partially reflected and transmitted into new waves as was shown in Fig. 8. The strength of the two new waves is determined by solving the propagation of a shock wave through a material discontinuity and imposing

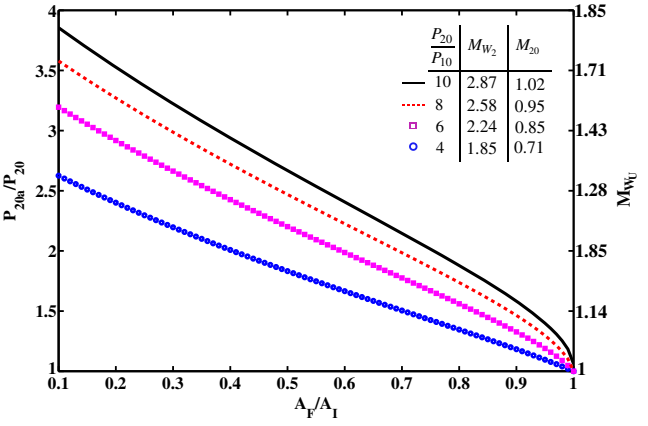

Fig. 10 Upstream-propagating wave strength as a function of area ratio for constant secondary shock strengths. Results are specific to helium gas.

that the resulting states across the reflected and transmitted waves satisfy the conditions $U_{5c} = U_{20b}$ and $P_{5c} = P_{20b}$ [34]. Finally, the portion of test gas that is contaminated by the transmitted wave is given by

$$t_c = \frac{L_{10} - \hat{x}}{W_T} - \frac{L_{10} - \hat{x}}{U_{5c}} \tag{2}$$

where L_{10} is the length of the expansion section, and U_{5c} is the speed of the flow in region (5c). W_T is the speed of the transmitted wave and is given by

$$W_T = U_5 - a_5\left[\frac{\gamma_5 + 1}{2\gamma_5}\left(\frac{P_{5\,c}}{P_5} - 1\right) + 1\right]^{1/2} \tag{3}$$

The quantity $\hat{x}$ is the distance from the secondary diaphragm at which the contact surface and the upstream-propagating wave intersect and can be computed as

$$\hat{x} = \frac{U_{20}L_{10}}{W_2} + U_{20}L_{10}\frac{W_2 - U_{20}}{W_2}\frac{1}{U_{20} + W_U} \tag{4}$$

W_2 is the secondary shock speed. By this analysis, we can infer that $U_{20b} < U_{20}$, and thus the speed of the contact surface has decreased.

This portion of the model was solved and the results are shown in Fig. 11. The peak contaminated test gas pressure and contaminated test time are given as a function of the disturbance wave strength. The peak pressure is normalized by the nominal test gas pressure when no disturbances are present. The contaminated test time t_c is normalized by the expansion section length because it was found to scale linearly with expansion section length, for a given M_{W_U}.

The analysis shows that if the disturbance has the strength of a Mach wave ($M_{W_U} = 1$), it does not alter the test gas pressure. However, the wave is still moving relative to the flow if U_{20} is subsonic, and therefore will penetrate through the test gas. As the strength of the disturbance increases, it penetrates through the contact surface a greater extent and alters the test gas pressure in the process.

C. Analysis of Model

Based on the outlined analysis, the peak contaminated test gas pressure and time are dependent on several experimental parameters; this dependence can be conveniently summarized as

$$(P_{5\,c}, t_c) = \tilde{F}\left(W_2, \frac{A_F}{A_I}, \gamma_{20}, \gamma_5, a_{20}, P_{20}, L_{10}\right) \tag{5}$$

The proposed model was used to predict the extent of the test gas interference effect for the two flow conditions studied experimentally. The results are summarized in Table 2, where the run number corresponds to that of Table 1. The results show that the model is capable of accurately predicting the extent of the interference effect

Table 2 Comparison of the experimental and modeling results

		$P_{5\,c}/P_5$		t_c/t_{total}	
Run number	A_F/A_I	Exp.	Model	Exp.	Model
2	0.79	2.1	2.1	0.49	0.55
4	0.82	2.3	2.1	0.62	0.57
6	0.82	1.5	1.8	0.17	0.11

The peak contaminated test gas pressure is normalized by the nominal test gas pressure when no interference effect is present. The contaminated test time is normalized by the experimentally measured total test time.

reasonably well considering the approximations that were made. Discrepancies between the experiments and model may be a result of several factors. First, the formation process of the disturbance wave requires some finite amount of time until it is fully developed and propagates at a nominal speed of W_U. In fact, the disturbance wave is the result of a series of compression waves that coalesce with one another and originate from each incremental change in area. Second, it may also be important to consider that the disturbance wave grows in size from an initial cross-sectional area of A_F to the entire area of the tube. This processes is not accounted for in the model. Third, the contact surface was modeled as a zero-thickness material discontinuity, which is not the case experimentally. The finite thickness of the contact surface will cause the interaction with the upstream propagating wave to be more complex in nature, where a series of transmitted and reflected waves are generated and eventually coalesce. Fourth, we conjecture that the effects of the boundary layer in state (20) have a negligible effect on the upstream propagating disturbance wave, which may not be the case in state ⑤. This conclusion is drawn from the measured static pressure in the expansion section of the tube. An example of a pressure trace acquired for flow condition A is given in Fig. 12, in which the location of the sensor is shown schematically in the figure inset. After the arrival of the secondary shock, the measured pressure of the shocked expansion gas in state (20) is constant, which suggests that no significant boundary-layer growth has occurred. On the other hand, the test gas in region ⑤ has traveled a significantly longer distance and has been processed by an expansion wave; thus, the boundary layer had a significantly longer time to grow. In this case, significant boundary-layer growth can be inferred by the observed increase in static pressure measured at a fixed point. Therefore, we expect that it is only when the transmitted wave penetrates through the contact surface that the boundary layer has an effect on any of the additional waves. A similar trend of the behavior of the boundary layer was observed in flow condition B as well as in flows generated in [18–20]. Thus, in general we use this as an indication that boundary-layer growth is negligible in state (20), but is present in state ⑤.

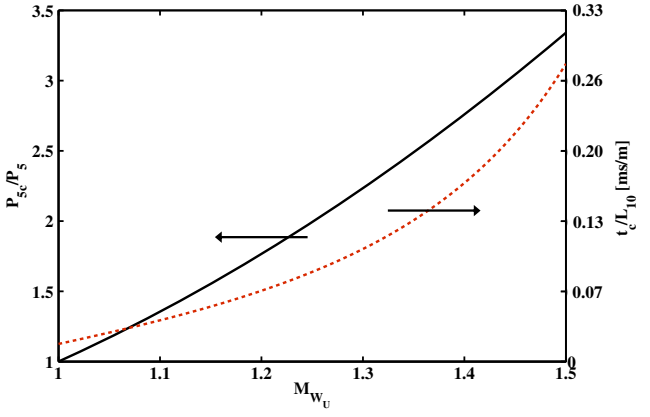

Fig. 11 Peak contaminated test gas pressure and contaminated test time as a function of upstream propagating wave strength.

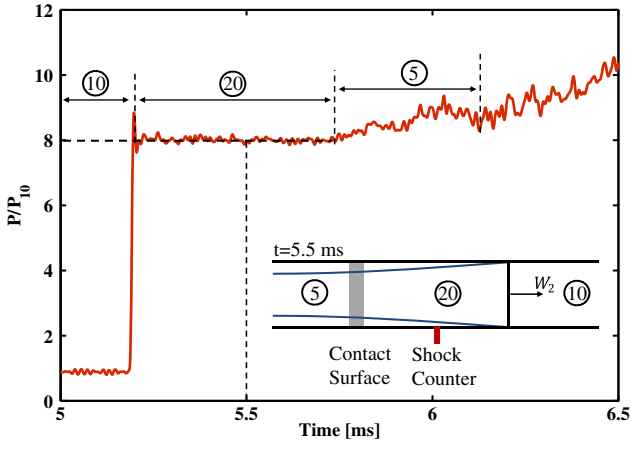

Fig. 12 Static pressure trace for flow condition A acquired 2.82 m downstream of the secondary diaphragm.

VI. Conclusions

This study has investigated the effects of test-article-induced interference on test gas properties in expansion tube flows through a series of experiments, numerical simulations and analytical considerations. This is a critical aspect to consider in expansion tube flows because of the limited size of the test gas core flow and test time in such facilities. The study conducted shows that a system of compression waves is generated and coalesce into an upstream-propagating disturbance wave as a result of the initial interaction of the secondary shock with the test model that partially blocks the expansion tube cross section. The disturbance wave has been shown to propagate upstream through the expansion gas and interact with the contact surface only to generate two new waves: a transmitted and a reflected wave. The transmitted wave partially penetrates the test gas, thus altering its aerothermodynamic properties. Furthermore, the speed of the contact surface is reduced.

Based on the present study, the interference effect can be accurately modeled to be a function of several parameters, which include the contraction area ratio and strength of the secondary shock wave. The effects of test gas interference are only suppressed if the test article is recessed into the test section. Based on the formulated model, any test model that protrudes into the expansion section and causes an area contraction will generate an upstream-propagating disturbance. Furthermore, this disturbance will always be strong enough to propagate upstream. More specifically, a secondary shock wave that has sufficient strength to generate a supersonic flow in state (20) will always generate an upstream-propagating disturbance, traveling at a speed W_U that is greater than U_{20}. A one-dimensional unsteady wave model was formulated to quantitatively predict the strength and temporal duration of the test gas interference and was found to accurately predict them for the range of flow conditions used in this study.

Acknowledgments

Yasin M. Abul-Huda acknowledges the support of the National Defense Science and Engineering (NDSEG) Fellowship as well as the Rackham Merit Fellowship (RMF). The part of this work conducted at Stanford University was performed under the auspices of the Department of Energy–sponsored Predictive Science Alliance Program (PSAAP) at Stanford University. The authors would like to thank an anonymous reviewer for inviting us to develop the model of Sec. V further into its current form.

References

[1] Trimpi, R., "Preliminary Theoretical Study of the Expansion Tube, a New Device for Producing High Enthalpy Short Duration Hypersonic Gas Flows," NASA TR-133, 1962.

[2] Shinn, J., and Miller, C., "Experimental Perfect-Gas Study of Expansion-Tube Flow Characteristics," NASA Technical Paper 1317, Vol. 1317, Dec. 1978.

[3] Paull, A., and Stalker, R., "Test Flow Disturbances in an Expansion Tube," *Journal of Fluid Mechanics*, Vol. 245, 1992, pp. 493–521. doi:10.1017/S0022112092000569

[4] Sasoh, A., Ohnishi, Y., Ramjaun, D., and Takayama, K., "Effective Test Time Evaluation in High-Enthalpy Expansion Tube Introduction," *AIAA Journal*, Vol. 39, No. 11, 2001, pp. 2141–2147.

[5] Dufrene, A., Sharma, M., and Austin, J. M., "Design and Characterization of a Hypervelocity Expansion Tube Facility," *Journal of Propulsion and Power*, Vol. 23, No. 6, Nov. 2007, pp. 1185–1193. doi:10.2514/1.30349

[6] McGilvray, M., Austin, J. M., Sharma, M., Jacobs, P. A., and Morgan, R. G., "Diagnostic Modelling of an Expansion Tube Operating Condition," *Shock Waves*, Vol. 19, No. 1, Feb. 2009, pp. 59–66. doi:10.1007/s00193-009-0187-9

[7] Paull, A., and Stalker, R. J., "The Effect on an Acoustic Wave as It Traverses an Unsteady Expansion," *Physics of Fluids*, Vol. 3, No. 4, 1991, p. 717. doi:10.1063/1.858079

[8] Wegener, M., Sutcliffe, M., and Morgan, R., "Optical Study of a Light Diaphragm Rupture Process in an Expansion Tube," *Shockwaves*, Vol. 10, No. 3, 2000, pp. 167–178.

[9] Furukawa, T., Aochi, T., and Sasoh, A., "Expansion Tube Operation with Thin Secondary Diaphragm," *AIAA Journal*, Vol. 45, No. 1, Jan. 2007, pp. 214–217. doi:10.2514/1.23846

[10] Miller, V. A., Gamba, M., Mungal, M. G., and Hanson, R. K., "Secondary Diaphragm Thickness Effects and Improved Pressure Measurements in an Expansion Tube," *AIAA Journal*, Vol. 52, No. 2, Feb. 2014, pp. 451–456. doi:10.2514/1.J052767

[11] Parziale, N. J., Rabinovitch, J., Blanquart, G., Hornung, H. G., and Shepherd, J. E., "Proposed Vertical Expansion Tunnel," *AIAA Journal*, Vol. 51, No. 12, Dec. 2013, pp. 2792–2799. doi:10.2514/1.J052389

[12] Maskell, E., "A Theory of the Blockage Effects on Bluff Bodies and Stalled Wings in a Closed Wind Tunnel," Aeronautical Research Council Reports and Memoranda, Vol. R&M 3400, 1963.

[13] West, G., and Apelt, C. J., "The Effects of Tunnel Blockage and Aspect Ratio on the Mean Flow Past a Circular Cylinder with Reynolds Numbers Between 10^4 and 10^5," *Journal of Fluid Mechanics*, Vol. 114, 1982, pp. 361–377. doi:10.1017/S0022112082000202

[14] Sudani, N., Valiferdowsi, B., and Hornung, H., "Test Time Increase by Delaying Driver Gas Contamination for Reflected Shock Tunnels," *AIAA Journal*, Vol. 38, No. 9, 2000, pp. 1497–1503. doi:10.2514/2.1138

[15] Stalker, R., "Driver Gas Contamination in a High-Enthalpy Reflected Shock Tunnel," AIAA Technical Note, 1978, pp. 277–279.

[16] Burtschell, Y., Cardoso, M., and Zeitoun, D., "Numerical Analysis of Reducing Driver Gas Contamination in Impulse Shock Tunnels," *AIAA Journal*, Vol. 39, No. 12, 2001, pp. 2357–2365. doi:10.2514/2.1242

[17] Heltsley, W., Snyder, J., Houle, A., Davidson, D., Mungal, M., and Hanson, R., "Design and Characterization of the Stanford 6 Inch Expansion Tube," AIAA Paper 2006-4443, 2006.

[18] Abul-Huda, Y., and Gamba, M., "Design and Characterization of the Michigan Hypersonic Expansion Tube Facility (MHExT)," AIAA Paper 2015-1785, Jan. 2015, pp. 1–13.

[19] Abul-Huda, Y., and Gamba, M., "Flow Characterization of a Hypersonic Expansion Tube Facility," *Journal of Propulsion and Power* (Under Review).

[20] Gamba, M., and Mungal, M. G., "Ignition, Flame Structure and Near-Wall Burning in Transverse Hydrogen Jets in Supersonic Crossflow," *Journal of Fluid Mechanics*, Vol. 780, 2015, pp. 226–273. doi:10.1017/jfm.2015.454

[21] McBridge, B., Gordon, S., and Reno, M., "Coefficients for Calculating Thermodynamic and Transport Properties of Individual Species," NASA TM-4513, 1993.

[22] Crist, S., Sherman, P. M., and Glass, D. R., "Study of the Highly Underexpanded Sonic Jet," *AIAA Journal*, Vol. 4, No. 1, 1966, pp. 68–71. doi:10.2514/3.3386

[23] Ashkenas, H., and Sherman, F., "Structure and Utilization of Supersonic Free Jets in Low Density Wind Tunnels," NASA CR-60423, Vol. 222, No. 45, 1962.

[24] Ben-Yakar, A., and Hanson, R. K., "Characterization of Expansion Tube Flows for Hypervelocity Combustion Studies," *Journal of Propulsion and Power*, Vol. 18, No. 4, 2002, pp. 943–952. doi:10.2514/2.6021

[25] Andronov, V., "Turbulent Mixing at Contact Surface Accelerated by Shock Waves," *Journal of Experimental and Theoretical Physics*, Vol. 44, No. 2, 1977, pp. 424–427.

[26] Dosanjh, D. S., and Sheeran, W. J., "Observations on Jet Flows from a Two-Dimensional, Underexpanded, Sonic Nozzle," *AIAA Journal*, Vol. 6, No. 3, 1967, pp. 540–542. doi:10.2514/3.4532

[27] Ben-Dor, G., Igra, O., Elperin, T., and Lifshitz, A., *Shock Wave Interaction and Propagation, Handbook of Shock Waves*, Vol. 2, Academic Press, Boston, 2001.

[28] Chester, B. W., "The Propagation of Shock Waves in a Channel of Non-Uniform Width," *The Quarterly Journal of Mechanics and Applied Mathematics*, Vol. VI, No. 4, 1953, pp. 440–452. doi:10.1093/qjmam/6.4.440

[29] Chisnell, R. F., "The Motion of a Shock Wave in a Channel, with Applications to Cylindrical and Spherical Shock Waves," *Journal of Fluid Mechanics*, Vol. 2, No. 3, 1957, pp. 286–298. doi:10.1017/S0022112057000130

[30] Whitham, G. B., "On the Propagation of Shock Waves Through Regions of Non-Uniform Area or Flow," *Journal of Fluid Mechanics*, Vol. 4, No. 4, 1958, pp. 337–360. doi:10.1017/S0022112058000495

[31] Russel, D., "Shock-Wave Strengthening by Area Convergence," *Journal of Fluid Mechanics*, Vol. 27, No. 2, 1967, pp. 305–314. doi:10.1017/S0022112067000333

[32] Bird, G., "The Effect of Wall Shape on the Degree of Reinforcement of a Shock Wave Moving into a Converging Channel," *Journal of Fluid Mechanics*, Vol. 5, No. 1, 1959, pp. 60–66. doi:10.1017/S0022112059000052

[33] Laporte, O., "On the Interaction of a Shock with Constriction," Univ. of California, Los Alamos Scientific Lab. Rept. LA-1740, 1954.

[34] Liepmann, H. W., and Roshko, A., *Elements of Gas Dynamics*, Wiley, New York, 1957, Chap. 2.

F. Alvi
Associate Editor